Supplementary Information

Electronic Structure and Band Gap Modulation of Ba–S Compounds via Tuned Hybrid Functional Calculations

Table S1 Optimized crystal structure of BaS_3 orthorhombic polymorph (lattice parameters).

Composition	Stoichiometry	Space Group (No.)	a (Å)	b (Å)	c (Å)	α (°)	β (°)	γ (°)
Ba_4S_{12}	BaS_3 (ortho.)	$P2_1\ 2_1\ 2_1$ (18)	8.6117	10.1373	5.1017	90	90	90

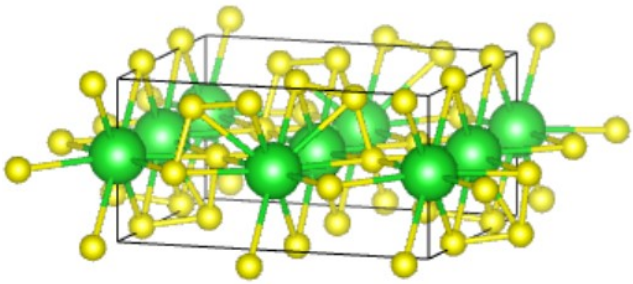

Figure S1: *Crystallographic diagram of BaS_3 orthorhombic polymorph (space group $P2_1\ 2_1\ 2_1$, No. 18). Large green and small yellow spheres represent Ba and S atoms, respectively.*

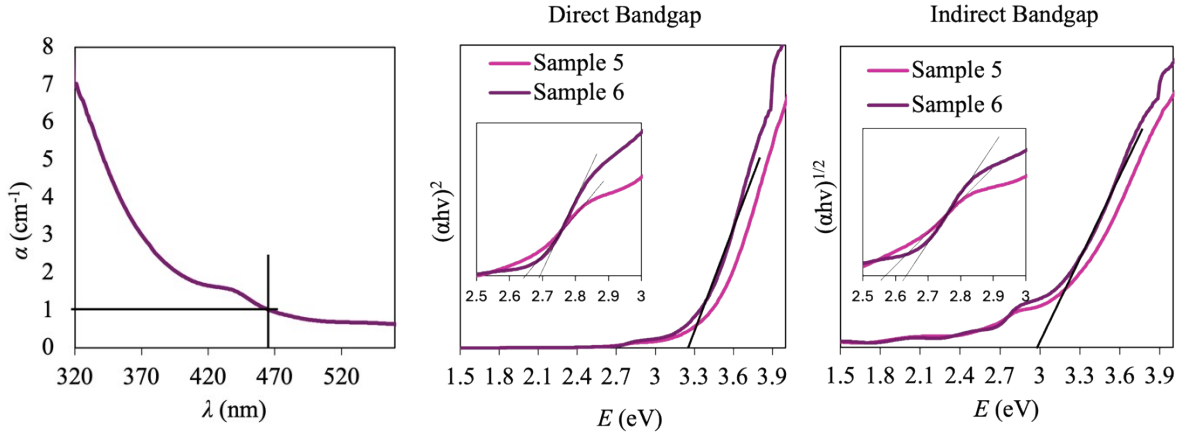

Figure S2: Absorption coefficient (α) as a function of wavelength for BaS_3 samples 5 and 6, used to verify the direct and indirect optical band gap assignments. The absorption onset near 470 nm is consistent with an indirect band gap, comparable to the absorption behavior of silicon included for reference.

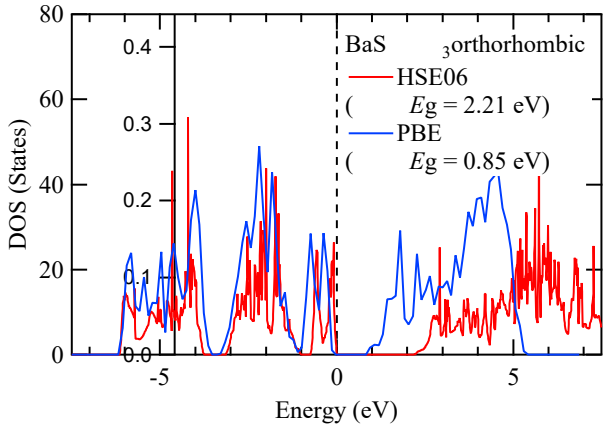

Figure S3. Total electronic density of states (DOS) for BaS_3 Orthorhombic calculated using the PBE (blue) and HSE06 (red) functionals Energies are referenced to the valence-band maximum (VBM = 0 eV, dashed line). Band gaps estimated from the DOS are BaS_3 (orthorhombic) = 2.21 eV (HSE06), 0.85 eV (PBE).

PBE Electronic Band Structures

To explicitly evaluate the nature of the electronic transitions and further justify the necessity of the HSE06 hybrid functional used in the main text, we calculated the electronic band dispersions of the Ba–S compounds along high-symmetry *k*-paths using the standard PBE functional.

As summarized in Table S2 and visualized in Figure S4, the standard semilocal PBE calculations predict a direct electronic transition (G-G) for cubic BaS. This theoretical prediction blatantly contradicts our experimental optical measurements (Tauc plot analysis), which indicate that BaS is fundamentally an indirect-gap semiconductor. This discrepancy—mischaracterizing an indirect gap as a direct gap—highlights the severe limitations of standard GGA functionals for these systems, where self-interaction errors distort the energy ordering of the band edges. Therefore, the computationally demanding HSE06 calculations discussed in the main text are strictly required to obtain an accurate description of the electronic structure consistent with the experimental observations.

Table S2. Summary of the electronic transitions for the Ba–S compounds calculated using the PBE functional.

Stoichiometry	VBM location	CBM location	Transition
BaS	Γ	Γ	Direct
BaS_2	L	Γ	In-direct
BaS_3 (tetra.)	Γ	Γ	Direct
BaS_3 (ortho.)	U	Z	In-direct

Figure S4. Electronic band dispersions of the Ba–S compounds calculated using the PBE functional along high-symmetry k-paths: (a) cubic BaS, (b) monoclinic BaS_2, (c) tetragonal BaS_3, and (d) orthorhombic BaS_3. The VBM is set to 0 eV.

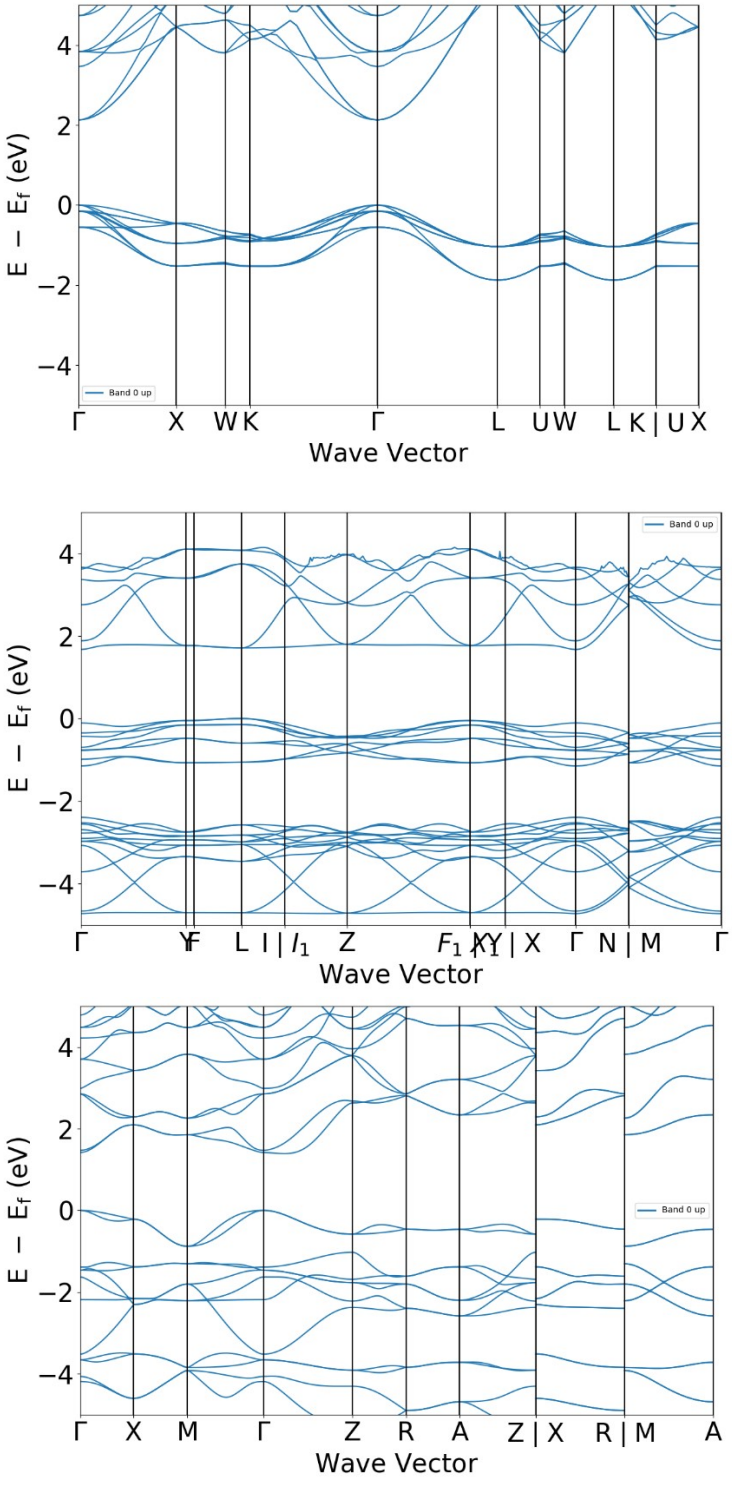

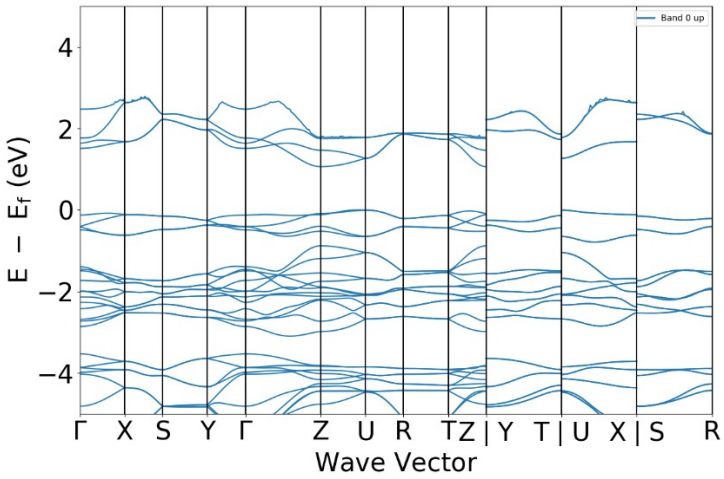

Sensitivity of Band Gaps to Lattice Parameter Variations

To evaluate the sensitivity of the electronic properties to minor structural deviations—such as standard functional-dependent lattice overestimation/underestimation or thermal expansion at room temperature—we calculated the band gaps of the Ba–S compounds under artificially applied ± 1 % uniform scaling to the lattice vectors (corresponding to approximately ± 3 % volume changes) using the standard PBE functional.

As summarized in Table S3, the band gap fluctuations for all phases are remarkably small (less than 0.06 eV) under both compressive (-1%) and tensile (+1%) strains. These minimal variations confirm that the semiconducting nature and the overall electronic picture of the Ba–S system discussed in the main text are highly robust and not critically sensitive to minor structural perturbations.

Table S3. Effect of ± 1 % uniform lattice scaling on the PBE band gap energies of the Ba–S compounds.

Stoichiometry	Gap at -1% strain (eV)	Gap at 0% strain (eV)	Gap at +1% strain (eV)	Maximum Variation
BaS	2.380	2.415	2.445	0.035
BaS_2	1.672	1.628	1.584	0.044
BaS_3 (tetra.)	1.675	1.618	1.576	0.042
BaS_3 (ortho.)	1.281	1.242	1.203	0.039

Projected Density of States (PDOS)

Figures S5–S7 present the projected density of states (PDOS) calculated using the PBE functional for BaS, BaS_2, and BaS_3 (tetragonal), respectively. The orbital decomposition confirms that the valence-band maximum (VBM) is dominated by S 3p states in all three phases, while the conduction-band minimum (CBM) is primarily derived from Ba 5d orbitals with minor Ba 6s contributions. In BaS_2 and BaS_3, the formation of S–S bonding units (S_2^{2-} dimers and S_3^{2-} trimers) introduces additional hybridized S 3p states near the VBM, directly responsible for the progressive narrowing of the band gap across the Ba–S series.

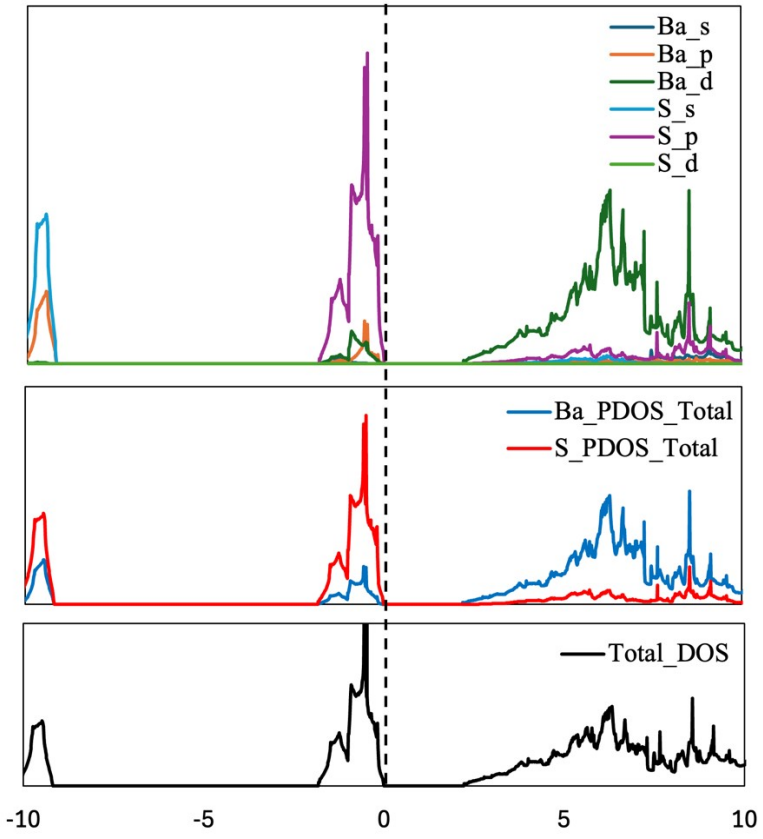

Figure S5. Projected density of states (PDOS) calculated using PBE for cubic BaS. Contributions from Ba 5d (green), Ba 6s (blue), and S 3p (red) orbitals are shown. The VBM is set to 0 eV.

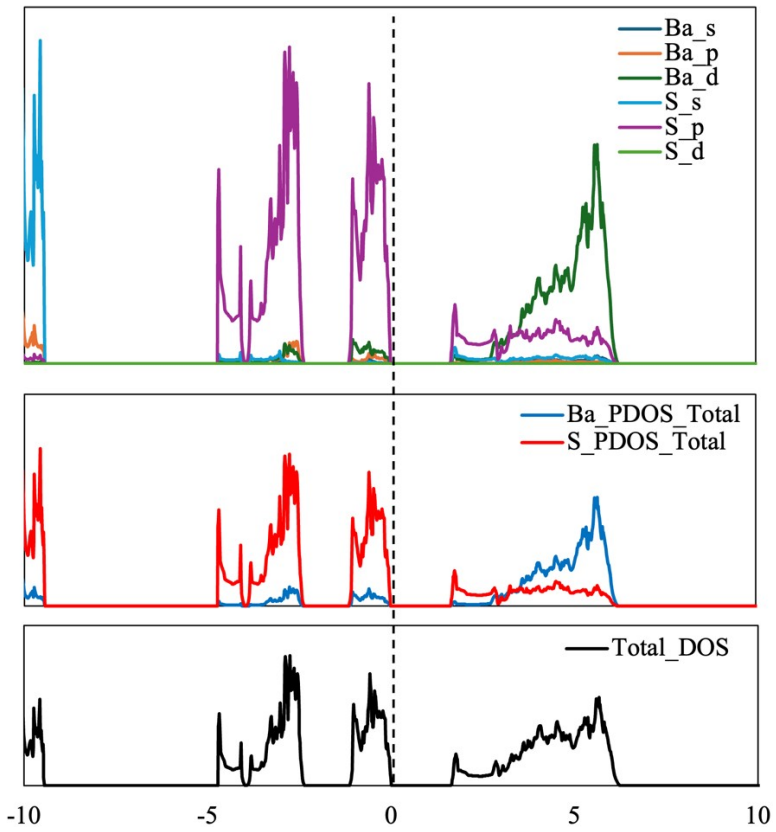

Figure S6. Projected density of states (PDOS) calculated using PBE for monoclinic BaS_2. Contributions from Ba 5d (green), Ba 6s (blue), and S 3p (red) orbitals are shown. The VBM is set to 0 eV. The enhanced S 3p contribution near the VBM compared to BaS reflects the presence of S_2^{2-} dimer units.

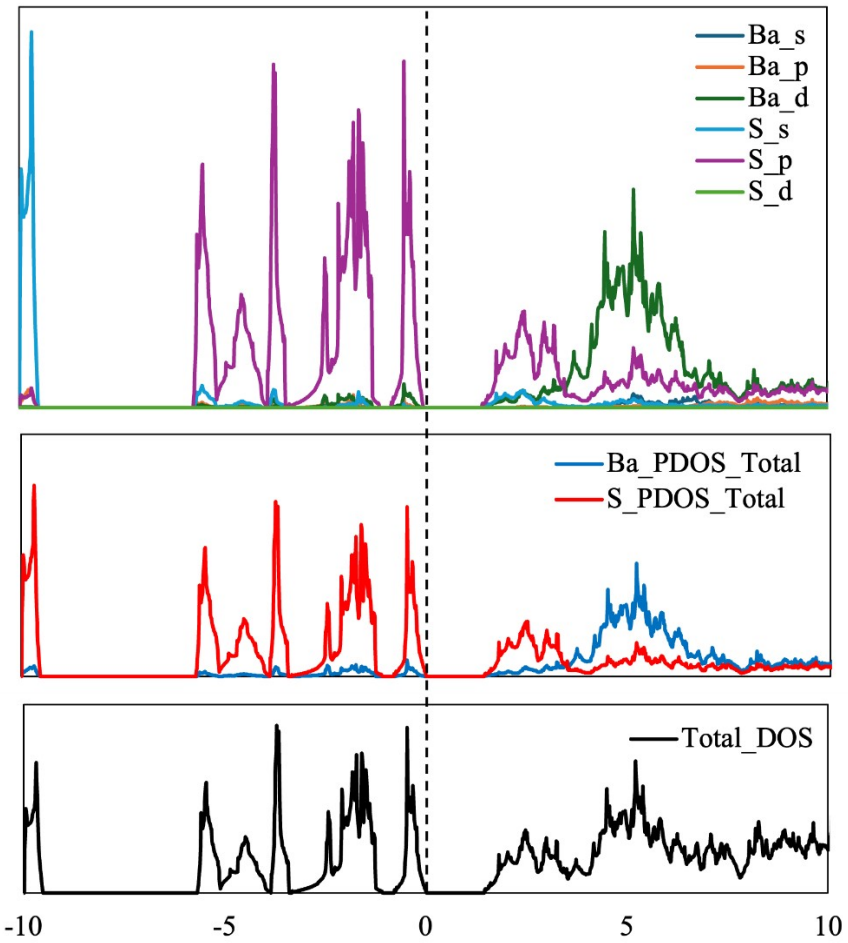

Figure S7. Projected density of states (PDOS) calculated using PBE for tetragonal BaS_3. Contributions from Ba 5d (green), Ba 6s (blue), and S 3p (red) orbitals are shown. The VBM is set to 0 eV. The further increase in S 3p states near the VBM relative to BaS and BaS_2 is consistent with the extended S_3^{2-} trimer coordination.

Calculated Optical Absorption Spectra (HSE06) and Comparison with Experiment

Figure S8 presents the optical absorption spectra calculated using the HSE06 hybrid functional for BaS, BaS_2, and BaS_3, shown alongside the corresponding experimental UV–Vis absorbance data. The calculated spectra were obtained from the imaginary part of the dielectric function $\varepsilon_2(\omega)$ computed at the HSE06 level on the PBE-optimized geometries.

The calculated absorption onsets are in good agreement with the experimental data for all three phases. Both the theoretical and experimental spectra confirm the systematic redshift in absorption edge from BaS to BaS_2 and BaS_3, consistent with the progressive narrowing of the band gap across the series. Minor discrepancies between the calculated and measured spectra are expected and arise from: (i) the Tauc method does not account for excitonic effects or disorder; (ii) HSE06 does not include excitonic contributions explicitly (as in Bethe–Salpeter equation calculations); and (iii) the calculated spectra assume ideal bulk periodicity, whereas the experimental films are polycrystalline and may contain defects or grain boundary effects.

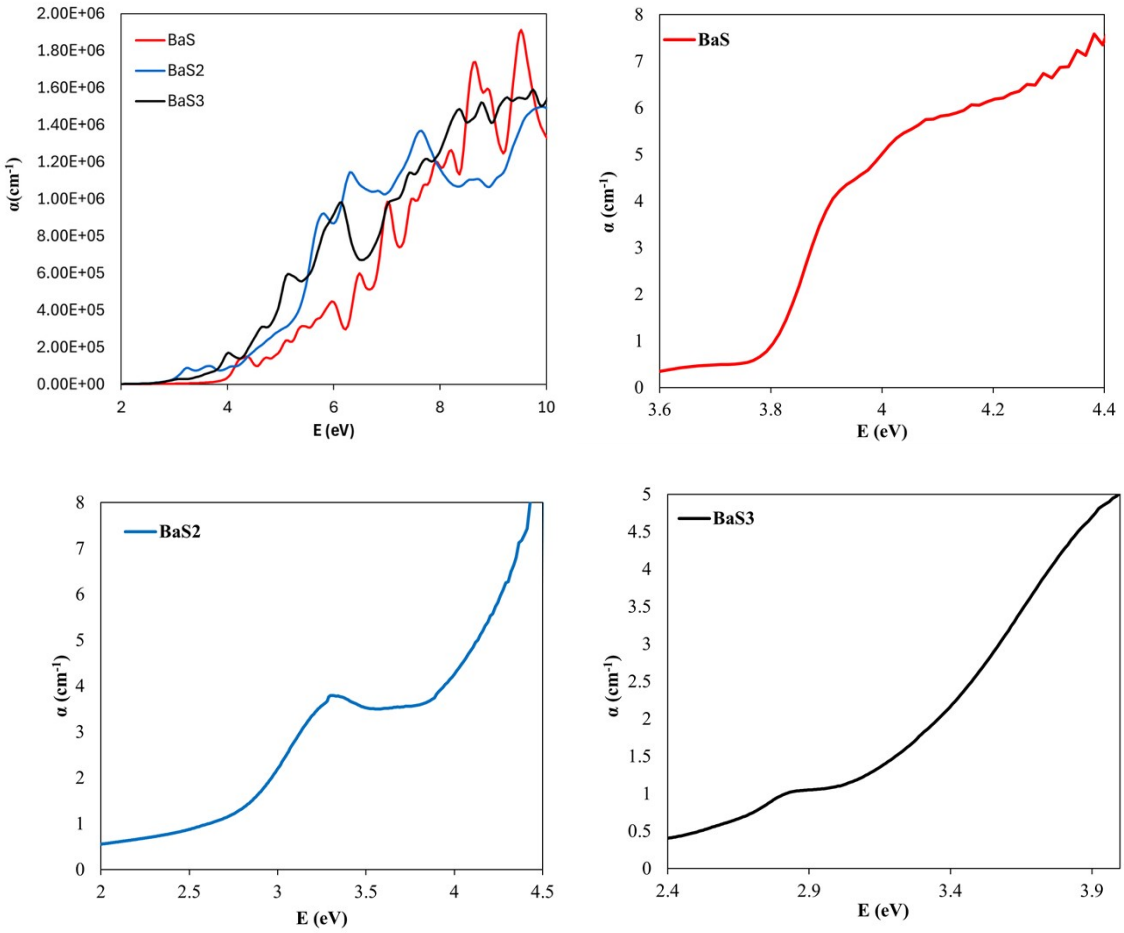

Figure S8. Comparison of calculated HSE06 optical absorption spectra (a), and experimental UV–Vis absorbance data (dashed lines) for (b) BaS, (c) BaS_2, and (d) BaS_3.

Effect of HFSCREEN Parameter on Calculated Band Gaps

Table S4 summarizes the HSE06-calculated band gaps for all three Ba–S phases as a function of the range-separation parameter μ (HFSCREEN), including the default value of μ = 0.20 $Å^{-1}$ as a baseline. This directly demonstrates that a single uniform μ value cannot simultaneously reproduce the experimental band gaps across all three phases, providing the physical motivation for the phase-specific μ values adopted in the main text.

Table S4. HSE06-calculated band gaps (eV) as a function of HFSCREEN parameter μ for BaS, BaS_2, and BaS_3 (tetragonal). Experimental values are included for comparison.

Phase	μ = 0.00 $Å^{-1}$	μ = 0.10 $Å^{-1}$	μ = 0.15 $Å^{-1}$	μ = 0.20 $Å^{-1}$ (default)	μ = 0.25 $Å^{-1}$	Experiment Direct gap (eV)	Experiment Indirect gap (eV)
BaS	3.8	—	—	3.1	—	3.8	3.8

BaS_2	—	—	—	2.8	2.7	2.9	2.7
BaS_3 (tetra.)	—	—	2.7	2.5	—	2.7	2.6

DFPT Results: Dielectric Constants and Born Effective Charges

The following tables present the density-functional perturbation theory (DFPT) results for the electronic dielectric constants and Born effective charges of all three Ba–S phases. These calculations were performed using VASP with the PBE functional and projector-augmented wave (PAW) pseudopotentials. Convergence with respect to the k-point mesh was verified by comparing results at two mesh densities for each phase (Table S5). All converged values are used in the discussion of electronic screening in the main text (Table 6).

Table S5. k-mesh convergence of DFPT calculations. Electronic dielectric constant (ε∞) and isotropic Born effective charges (Z) computed at two k-mesh densities for each phase. All calculations performed with VASP using the PBE functional. Converged (dense) values are used throughout the main text.*

Compound	Structure	k-mesh	ε∞	Z*(Ba) / e	Z*(S) / e
BaS	Rocksalt ($Fm\bar{3}m$)	6×6×6	4.806	+2.609	−2.609
BaS	Rocksalt ($Fm\bar{3}m$)	8×8×8	4.809	+2.609	−2.609
BaS_2	Monoclinic C2/c	5×5×5	4.965	+2.654	−1.327
BaS_2	Monoclinic C2/c	7×7×7	4.969	+2.654	−1.327
BaS_3	Tetragonal $P\bar{4}2_1m$	4×4×6	5.906	+3.017	see Table S6
BaS_3	Tetragonal $P\bar{4}2_1m$	6×6×8	5.924	+3.017	see Table S6

Table S6. Born effective charges for all inequivalent atoms (dense k-mesh). Atom-resolved Born effective charges Z (isotropic average) from the converged DFPT calculations. Nominal ionic charges are given for comparison; ΔZ* = Z* − Z_nominal reflects covalency and dynamical charge transfer. The acoustic sum rule (∑Z* = 0 per unit cell) is satisfied in*

all cases. Note: the anomalous positive Z on the apical S site in BaS_3 reflects strong hybridisation with Ba 5d states.*

Compound	Atom	Species	Z* / e	Nominal / e	ΔZ* / e
BaS	1	Ba	+2.609	+2	+0.609
BaS	2	Ba	+2.609	+2	+0.609
BaS	3	Ba	+2.609	+2	+0.609
BaS	4	Ba	+2.609	+2	+0.609
BaS	5	S	−2.609	−2	−0.609
BaS	6	S	−2.609	−2	−0.609
BaS	7	S	−2.609	−2	−0.609
BaS	8	S	−2.609	−2	−0.609
BaS_2	1	Ba	+2.654	+2	+0.654
BaS_2	2	Ba	+2.654	+2	+0.654
BaS_2	3	Ba	+2.654	+2	+0.654
BaS_2	4	Ba	+2.654	+2	+0.654
BaS_2	5–12	S	−1.327	−2	+0.673
BaS_3	1	Ba	+3.017	+2	+1.017
BaS_3	2	Ba	+3.017	+2	+1.017
BaS_3	3–6	S (bridging)	−1.549	−2	+0.451
BaS_3	7–8	S (apical)	+0.081	−2	+2.081

Table S7. Summary of converged DFPT parameters. Electronic dielectric constant (ε∞, isotropic average) and acoustic sum rule (ASR) verification for all three phases. ∑Z is the sum of all Born effective charges in the unit cell.*

Compound	k-mesh	Space group	ε∞ (avg)	∑Z* / e	ASR
BaS	8×8×8	$Fm\bar{3}m$ (225)	4.809	0.000	Satisfied
BaS_2	7×7×7	C2/c (15)	4.969	0.000	Satisfied
BaS_3	6×6×8	$P\bar{4}2_1m$ (113)	5.924	0.000	Satisfied

Computational Details for DFPT

All DFPT calculations were performed with VASP using the PBE exchange-correlation functional and projector-augmented wave (PAW) pseudopotentials. The electronic dielectric tensor and Born effective charges were computed via density-functional perturbation theory (DFPT). Monkhorst–Pack k-point grids were used throughout. Convergence was assessed by comparing results at the standard and dense k-meshes listed in Table S5; differences in ε∞ are ≤0.3% and Born effective charges are unchanged to three decimal places, confirming full convergence. The acoustic sum rule (∑Z* = 0 per unit cell) is satisfied for all phases, as verified in Table S7.